Line profile of H Lyman-β emission from dissociative excitation of H_2

Joseph M. Ajello, Syed M. Ahmed, and Xianming Liu
Jet Propulsion Laboratory, California Institute of Technology, Pasadena, California 91109
(Received 28 July 1995)

A high-resolution ultraviolet spectrometer was employed for a measurement of the H Lyman-β (H L_β) emission Doppler line profile at 1025.7 Å from dissociative excitation of H_2 by electron impact. Analysis of the deconvolved line profile reveals the existence of a narrow central peak, less than 30 mÅ full width at half maximum (FWHM), and a broad pedestal base about 260 mÅ FWHM. Analysis of the red wing of the line profile is complicated by a group of Werner and Lyman rotational lines 160–220 mÅ from the line center. Analysis of the blue wing of the line profile gives the kinetic-energy distribution. There are two main kinetic-energy components to the H($3p$) distribution: (1) a slow distribution with a peak value near 0 eV from singly excited states, and (2) a fast distribution with a peak contribution near 7 eV from doubly excited states. Using two different techniques, the absolute cross section of H L_β is found to be $3.2\pm0.8\times10^{-19}$ cm^2 at 100-eV electron impact energy. The experimental cross-section and line-profile results can be compared to previous studies of Hα (6563.7 Å) for principal quantum number $n=3$ and L_α (1215.7 Å) for $n=2$.

PACS number(s): 34.80.Gs, 33.50.Dq

INTRODUCTION

For many years high-resolution studies in the visible region of the spectrum have been carried out on the Balmer series (principal quantum number, $n=3$, 4, and 5 excited states) of H produced by dissociative excitation of H_2 upon electron impact. For each principal quantum number, two major sets of kinetic-energy distributions were found, corresponding to the ''slow'' and ''fast'' distributions with typical kinetic energies of near 0 and 4–10 eV, respectively. The principal architects of these measurements were Ogawa, Ito, and co-workers [1–3]. They have carefully shown that the two kinetic-energy distributions reflect effects of dissociation from singly excited bound states (slow component) and from repulsive doubly excited states (fast component). Recently, we have begun high-resolution studies of the Lyman series of H from dissociative excitation of H_2 [4,5], utilizing a high-resolution 3-m vacuum ultraviolet (vuv) spectrometer with a resolving power of greater than 50 000 [6]. We reported a measurement of the H Lyman-α (H L_α) emission Doppler profile from dissociative excitation of H_2 by electron impact. Analysis of the deconvolved line profile revealed the existence of a narrow central peak of 40 ± 4 mÅ full width at half maximum (FWHM) and a broad pedestal base about 240-mÅ-wide FWHM. Slow H($2p$) atoms with peak energy near 80 meV produce the peak profile, which is nearly independent of impact energy. The wings of H L_α arise from dissociative excitation of a series of doubly excited Q_1 and Q_2 states, which define the core orbitals. The energy distribution of the fast atoms shows a peak at about 4 eV. In this work we extend the measurements to the $3p$ state and compare our results to line-profile studies of H_α. The H_α line profile shows a characteristic narrow central peak (~300-mÅ FWHM) from the slow component and a broad wing (~1.8-Å FWHM) from the fast component in the optical region. Since the Doppler displacement is proportional to wavelength, six-times narrower line profiles can be expected in the vacuum ultraviolet spectral region for the Lyman series.

It is also a goal of this study to directly measure the absolute cross section for H L_β at 100 eV for completely modeling the H_2 vacuum ultraviolet spectrum for both calibration and astronomy purposes. Once before, in 1984, we have applied published H_α absolute cross-section results [7] to a low-resolution H_2 vuv spectrum from our laboratory to determine the absolute H L_β cross section [8].

The most important application of the Lyman series line profiles is the opportunity to study and distinguish the emission spectrum of hydrogen from its molecular and atomic forms. The advent of high-resolution spacecraft such as the Hubble space telescope (HST), equipped with the Goddard high-resolution spectrograph and the planned astrophysical extreme ultraviolet observatories, have led to the measurement of the H L_α line profile in both the auroral zones and the dayglow of the planet Jupiter. H L_α line-profile wings extending to ±1 Å from line center have been measured in the aurora by the HST, and line core widths of greater than 140 mÅ have been observed by International ultraviolet explorer [9,10]. The primary cause of the dayglow in the Lyman series is a combination of resonant scattering of the solar emission line by atomic H and photoelectron dissociative excitation of H_2, the principal atmospheric constituent. Each process produces a broad line profile from multiple scattering in an optically thick upper atmosphere of atomic H. The main cause of the aurora is primary particle bombardment by electrons, protons, and heavier ions, followed by secondary electron excitation of the Lyman series. The large amount of Lyman and Werner band emissions ensures that dissociative excitation of H_2 is an important process.

EXPERIMENT

The experimental system has been described by Liu *et al.* [6]. In brief, the experimental system consists of a high-resolution 3-m uv spectrometer in tandem with an electron-impact collision chamber. For the H L_β line profile, a resolving power of 27 000 is achieved by operating the spectrometer in second order. The H L_α line profile has been

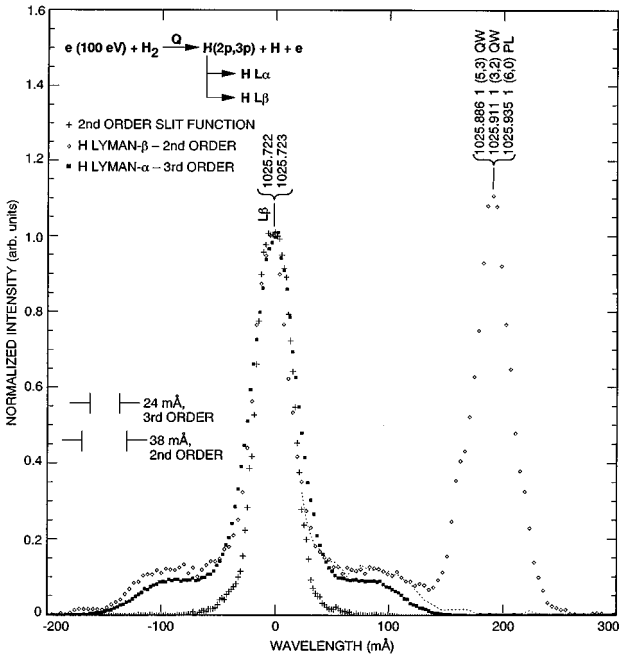

FIG. 1. Overplot of experimental spectra: 100-eV H L_β line profile in second order (open diamonds); 100-eV H L_α line profile in third order (filled squares); zero-order slit function of experimental apparatus scaled to second order (plus signs). The data statistics were better than 2.5%. The wavelength step size in second order was 4 mÅ and in third order 2.667 mÅ. The operating conditions were established as follows: (1) background gas pressure of 2.3×10^{-4} torr and (2) electron-beam current of 130 A. Peak signal was 4 000 and 13 000 counts in the 100-eV H L_β and H L_α line profiles, respectively, with background signals of under 100 counts.

previously reported [4,5] and was measured in third order at a resolving power of 50 000. The line shapes were measured with experimental conditions that ensure linearity of signal with electron-beam current and background gas pressure. In this study the line-profile spectra were measured in the crossed-beam mode, and the one low-resolution H L_β excitation function was obtained in the static gas mode. The operating conditions for the collision chamber included an electron-beam current of 130 μA and an H_2 gas pressure of 2.3×10^{-4} torr. The electron-impact-induced-fluorescence line profiles of H L_α and H L_β at 100-eV impact energy are shown in Fig. 1, along with the instrumental slit function of the spectrometer in second order. It is found that the H L_β line profile has a red wing that is blended by three moderately strong Lyman (L) and Werner (W) rotational lines, detailed in Table I, among other rotational lines in the neighborhood of the red wing of H L_β. One of the three strong lines is the L $1(6,0)P$ resonance line, lying furthest from H L_β line center. The closest, the W $1(5,3)Q$ rotational line, lies 163 mÅ from H L_β line center. We estimate the extent of the red wing by reflecting the blue wing about line center. It is shown as a dashed line in Fig. 1. The major wing of the H L_β line profile extends 150 mÅ from line center. A very weak secondary pedestal wing extends to 175 mÅ from line center. By comparison the H L_α wing extends 140 mÅ (reported FWHM=240 mÅ) from line center [4,5]. The Doppler wavelength shift is proportional to the rest wavelength. Much greater kinetic energies are released during $n=3p$ dissociation than for $n=2p$ dissociation to account for the broader H L_β line profile.

The weak signal from H L_β in third order prompted the second-order study. Yet note that the line core FWHM is nearly (40 vs 38 mÅ) at the limit of the second-order slit function. It is slightly narrower than the third-order line core profile from H L_α, even though the H L_α slit function was a narrow 24 mÅ that is indicated in Fig. 1. For this reason it will not be possible to accurately determine the slow atom distribution function as we were able to do for H L_α [4,5].

H L_β CROSS SECTION AT 100 eV

The first step in our comparative study of H L_α and H L_β was to measure the absolute cross section of H L_β at 100 eV. We can find the cross section by two methods. One method relies on the absolute cross section of H L_α at 100 eV, together with a relative calibration of H L_α and H L_β line intensities; the other method uses the absolute cross sections of the three major L & W features in the red wing of H L_β.

For the first method, the cross section of H L_α has been measured to be 7.3×10^{-18} cm^2 at 100 eV [11]. The relative sensitivity calibration in the vuv at 100 eV, using the H_2 ''many-line'' spectrum, has been described in fine structure [6,11]. The two-step process involved (1) measuring the H L_β to H L_α intensity ratio at 100 eV and (2) determining the relative calibration between 1025 and 1216 Å. The sensitivity calibration was performed in second order using the synthetic vuv line intensities of Liu *et al.* [6], convolved to the same resolution as the experimental low-resolution spectrum. The approximately 16 continuous 25-Å wide spectral regions provided a smooth calibration curve between 900 and 1300 Å. A typical vuv calibration curve is shown in Liu *et al.* [6]. By applying this first method, the ratio of cross sections was determined to be $Q(\mathrm{H}\ L_\beta)/Q(\mathrm{H}\ L_\alpha)=0.0412$ at 100 eV. $Q(\mathrm{H}\ L_\beta)$ is $(3.0\pm0.8)\times10^{-19}$ cm^2.

The second method gave an independent evaluation of the cross section. It is also a method that is free of instrument calibration. We have recently measured the L & W fine-structure direct cross-section energy dependence from 0–1 keV [25]. Using the oscillator strengths of Abgrall *et al.* [12–14], we are able to place on an absolute scale the cross section for every rotational line at 100 eV. The three strong L & W rotational lines found in the red wing of the H L_β line are shown in Table I, along with corresponding intensities. The $1(6,0)P$ L rotational line required ~40% correction for optical depth at the measurement pressure of 2.3×10^{-4} torr and the path length of foreground gas of 11.05 cm. The fractional L & W area of the total blended L_β+L & W feature in Fig. 1 is 42.4%. The ratio of $Q(L_\beta)$ to Q(L & W) is 1.36. At 100 eV, we find the cross section of H L_β to be $3.4\pm0.8\times10^{-19}$ cm^2 after subtracting a weak residual molecular contribution within the L_β profile. The average cross section of H L_β at 100 eV based on these two methods is $3.2\pm0.8\times10^{-19}$ cm^2. The total cross section of the blended feature in Fig. 1 is $(5.6\pm1.4)\times10^{-19}$ cm^2.

KINETIC-ENERGY DISTRIBUTION OF FAST PRODUCTS

The determination of the kinetic-energy distribution of the products is a two-step process that we have described in the

TABLE I. H_2 emission spectral intensities near H Lyman-β transition.

Wavelength (Å)	Intensity[a]	Relative intensity	Assignment[b]
1025.880	3.0490×10^{-2}	2.1256×10^{-3}	2(10, 5) *P* Werner
1025.886	4.6709	3.2563×10^{-1}	1(5, 3) *Q* Werner
1025.888	8.6408×10^{-19}	6.0240×10^{-20}	13(13, 0) *R* Lyman
1025.895	2.3861×10^{-4}	1.6635×10^{-5}	4(11,11) *Q D*
1025.911	1.4344×10^{1}	1.0000	1(3, 2) *Q* Werner
1025.918	8.3739×10^{-8}	5.8379×10^{-9}	8(2, 5) *Q D*
1025.922	1.0748×10^{-7}	7.4930×10^{-9}	6(11, 5) *R* Werner
1025.935	7.3617	5.1323×10^{-1}	1(6, 0) *P* Lyman
1025.936	6.8840×10^{-3}	4.7992×10^{-4}	3(10, 5) *R* Werner
1025.957	5.9106×10^{-2}	4.1206×10^{-3}	3(24, 4) *P* Lyman
1025.961	5.1620×10^{-8}	3.5987×10^{-9}	8(4, 2) *Q* Werner
1025.974	4.3545×10^{-9}	3.0358×10^{-10}	7(36, 5) *P* Lyman
1025.998	5.8953×10^{-5}	4.1099×10^{-6}	6(5, 5) *R B′*
1026.016	2.2821×10^{-10}	1.5910×10^{-11}	7(35, 5) *R* Lyman
1026.019	8.7148×10^{-2}	6.0756×10^{-3}	1(14, 2) *P* Lyman
1026.072	1.3969×10^{-13}	9.7386×10^{-15}	10(19, 2) *R* Lyman
1026.079	3.5100×10^{-1}	2.4470×10^{-2}	3(3, 6) *Q D*
1026.096	5.1721×10^{-5}	3.6058×10^{-6}	3(16,14) *Q D*
1026.099	5.1928×10^{-4}	3.6202×10^{-10}	10(1, 3) *P B′*

[a]Effective intensities (unit: 10^{-20} photons per H_2 molecule).

[b]Transition is labeled by $J''(v',v'')\Delta J$. Lyman, Werner, B', and D refer to $2p\sigma\ B\ ^1\Sigma_u^+\leftrightarrow X\ ^1\Sigma_g^+$, $2p\pi\ C\ ^1\Pi_u\leftrightarrow X\ ^1\Sigma_g^+$, $3p\sigma\ B'\ ^1\Sigma_u^+\leftrightarrow X\ ^1\Sigma_g^+$, and $3p\pi\ D\ ^1\Pi_u\leftrightarrow X\ ^1\Sigma_g^+$ electronic transitions, respectively.

previous paper on H L_α [4,5]. The resolution of the experiment is not sufficient to recover the slow distribution of $H(3p)$ atoms. However, the width of the wings is broad with respect to the instrument slit function. On this basis it is possible to locate the peak of the kinetic-energy distribution function of fast $H(3p)$ and estimate the shape of the distribution function. The measured line profile is the convolution of the true line profile and the instrumental slit function. Expressed mathematically the measured line profile, $I(\lambda)$, is given by the convolution integral

$$I(\lambda)=\int T(\lambda')A(\lambda-\lambda')d\lambda', \tag{1}$$

where $T(\lambda')$ is the true line profile at wavelength λ', and $A(\lambda-\lambda')$ is the instrumental response function. In the transform domain the convolution becomes a simple product,

$$I_T(s)=T_T(s)A_T(s), \tag{2}$$

where I_T, T_T, and A_T are the fast-Fourier transform (FFT) of I, T, and A, respectively, and s is measured in inverse wavelengths. Optimal Wiener filtering of the measured signal I was performed, since it includes a small noise component [15]. The signal-to-noise ratio (S/N) is greater than 40 for all line profiles. The FFT of T is given by

$$T_T(s)=I_T(s)F_T(s)/A_T(s), \tag{3}$$

where $F(\lambda)$ is the optimal filter. We selected a $\cos^{40}(s)$ to remove high-frequency noise from the ratio of I_T to A_T. We show in Fig. 2 the inverse FFT of $T_T(s)$ for the 100-eV line profiles of H L_α and H L_β compared to the wavelength scaled H_α results of Freund, Schiavone, and Brader *et al.* [16] and Higo, Komata, and Ogawa *et al.* [2]. The L_β feature arises from a single multiplet corresponding to the transition $1s$-$3p$. However, the H_α feature consists of three multiplets from the transitions $2s$-$3p$, $2p$-$3s$, and $2p$-$3d$. Only the first H_α multiplet ($2s$-$3p$) shares the same upper level. For that H_α multiplet the line profile would be identical to L_β when scaled in wavelength by the factor 1025.7/6563.7, according to the Doppler principle. In the comparison in Fig. 2, we have assumed that all three multiplets produce the same line profile. This is plausible since their $3l$ dissociation asymptotes are degenerate.

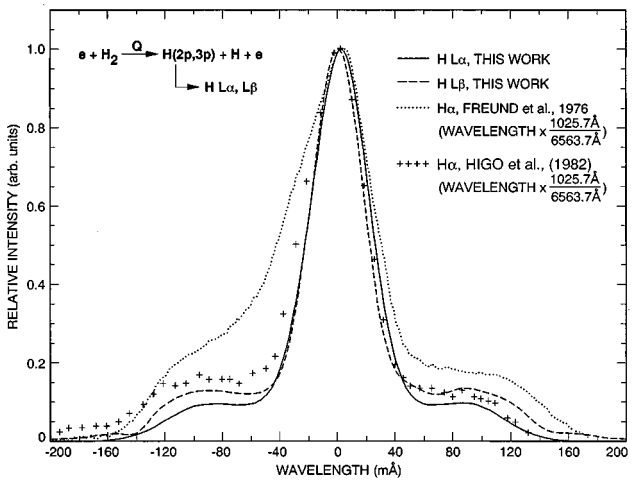

FIG. 2. Deconvolution of the 100-eV line-profiles data of H L_β (solid line) and H L_α (dashed line) of Fig. 1, along with a comparison to published data of H_α line profiles.

The first interpretation from Fig. 2 comes from a comparison of the 100-eV line profiles of H L_α and H L_β. The wings of the H L_β line profile are broader and more intense than those of H L_α. The FWHM of H L_α is 240 mÅ, while the H L_β line profile has a FWHM of 260 mÅ. The ratio of the two FWHM (L_β to L_α) is a modest 1.08. This ratio can be used to find the ratio of the average kinetic energy for fast H($3p$) and H($2p$) atoms. The ratio is made larger by an additional factor of 1.41 when converting the Doppler shifts to an equivalent translational energy. More details on the energy dependence of the distribution are discussed below. As described earlier, we were only able to measure an unblended line profile for the blue wing of H L_β. We have assumed that the red wing is identical. Since the H_α line is slightly asymmetric, the same can be expected to be true of H L_β. The comparison of the H L_β line profile with the two published H_α line profiles is in quite good agreement with the results of Higo *et al.* [2] and verified recently by Ogawa *et al.* [3]. The comparison with Freund *et al.* [16] is quite poor. Those authors have pointed out that their H_α line profiles were flawed by spectrometer aberrations. Note that the H_α line profile of Higo *et al.* [2] and the L_β line profile indicate the appearance of a weak secondary wing extending to nearly 200 mÅ from L_β line center. The initial indication from our data is that the line core of H L_α is broader than for H L_β. In Fig. 1, at the lower resolution afforded by second order for H L_β, we find a narrower line than for H L_α. This result can be attributed to the energy scale relating to the processes for production of slow H($2p$) atoms from direct excitation, cascade, and predissociation, particularly the last [4,5,17,18]. We place an upper limit of 30 mÅ on the FWHM of H L_β compared to our previously reported value of 40 mÅ for H L_α.

For the 100-eV line profile, the kinetic-energy distribution of the fragments, $P(E)$ is given by

$$P(E)=k(dT/d\lambda), \tag{4}$$

where k is a multiplicative constant [19]. With this approach, the 100-eV electron-impact line profiles for H L_α and H L_β in Fig. 2 were differentiated. The combined kinetic-energy distributions of the fast and slow H($2p$) and H($3p$) fragments are shown in Fig. 3 for the blue wing of H L_α and H L_β. The results for the H($3p$) atom distribution show a peak kinetic energy at 7 eV compared to the H($2p$) peak near 4 eV. The high-energy end of the kinetic-energy distribution indicates that the dissociation process releases pairs of H atoms with 10-eV energy per atom. The low end of the distribution begins at about 1 eV. We have previously shown that the H($2p$) distribution changes with electron-impact energy. A comparison of the results for H($3p$) at 100 eV with those of Ogawa, Ito, and co-workers is excellent. For example, their first measurement [1] of H($3l$) kinetic-energy distribution from H_α line-profile studies showed two kinds of kinetic-energy distributions, an average kinetic energy of 7 eV associated with the fast group and an average kinetic energy of 0.3 eV attributed to the slow group. More detailed analysis of the Balmer series by Higo *et al.* [2] followed. They measured the line profiles for H_α, H_β, and H_γ. At an electron-impact energy of 100 eV, the translational energy distributions had a fast peak at 7–8 eV and a slow peak at ~0 eV.

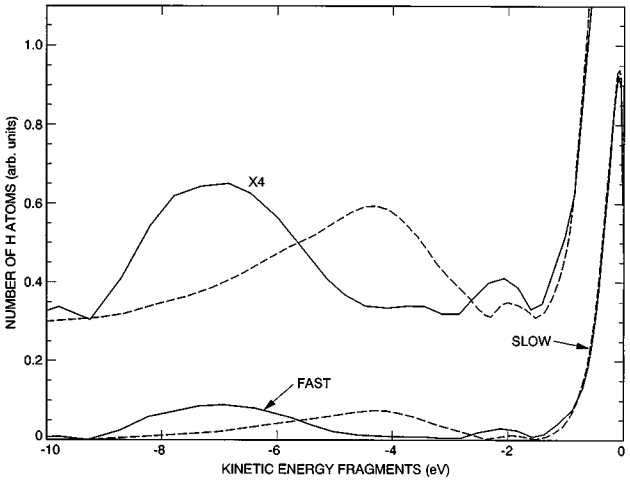

FIG. 3. Fast H($3p$) and H($2p$) atom kinetic-energy distribution functions. The solid line refers to H($3p$) and the dashed line to H($2p$).

The high-kinetic energy fragments result from dissociation through a series of repulsive curves that involve doubly excited electron orbitals. These doubly excited states have been described by Guberman [20]. The Q_1 Rydberg series of states consist of a $2p\sigma_u$ core orbital plus excited states of u symmetry. These repulsive states converge to the $^2\Sigma_u^+$ state of H_2^+. The Q_2 Rydberg series of states consist of a $2p\pi_u$ core orbital plus excited states. These repulsive states converge to the $^2\Pi_u$ state of H_2^+. Guberman [20] has shown that the potential curves of the manifold of Q_1 states are steeper in the Franck-Condon region than the Q_2 states and lead to 7 eV per atom upon H_2 dissociation. The potential curves of the mainfold of Q_2 states, being less steep, result in a kinetic-energy distribution with a peak near 4 eV per atom.

At 100-eV impact energy, both the Q_1 and Q_2 states can contribute to the approximately 14 eV of kinetic energy released to the pair of excited H atoms at the peak of the $3p$ kinetic-energy distribution in Fig. 3. However, in the threshold energy range, the Q_1 state is the only source of fast H atoms between 23- and 30-eV impact energies [4,5], and as pointed out above, the Q_1 state remains the dominant source of H($3p$) at all electron-impact energies. The lowest Q_1 $[^1\Sigma_g^+(1)(2p\sigma_u)^2]$ state crosses the Franck-Condon region at 23 eV. In our case, a curve crossing of this doubly excited state via homogeneous perturbation with the dissociating state $(1s\sigma_g)(3l)$ (16.67-eV dissociating energy) leads to the first group of fast H atoms for $n=3$. It is important to note, on the other hand, that the Q_2 states are dominant for H($2p$) above 30-eV electron-impact energy. The difference between the two processes can be attributed to the behavior of the Q_1 asymptotes of the potential curves at large internuclear distances (2–4 Å). Many of the Q_1 states have a potential curve with a potential minimum above the H($1s$)+H($2l$) dissociation limit but below the H($1s$)+H($3l$) dissociation limit. Thus, more Q_1 states are available for H($3p$) production [26].

Ogawa and co-workers have carefully measured the central peak of the H_α line profile. They find the central peak of the H_α line profile to have a FWHM of 0.32 Å at 100-eV impact energy. They also find the central peak to be asymmetric because of fine structure. They find the same results

as illustrated here from the point of view of line-profile and kinetic-energy distribution in Fig. 2 and Fig. 3, respectively, for the ratio of the fast-to-slow component H atom intensities. The relative intensity of fast atoms increases with increasing principal quantum number. For $H=2p$ we found that 31% of the atoms released in the dissociation processes are fast [4,5]. Integrating under the kinetic-energy distribution curve for $H=3p$ in Fig. 3, we find that 47% of the atoms expelled in the dissociation process are fast. On a qualitative basis the line-profile comparisons in Fig. 2 show the same results. If we take the central core FWHM reported by Ito *et al.* [1] and divide by six, we would predict that the H L_β central core should be 50 mÅ FWHM. On the other hand, our results suggest a FWHM of less than 30 mÅ. The difference may be ascribed to the lack of resolution in the H_α measurements to separate all the fine-structure components. The complex line at 6562.8 Å is composed of three multiplets at 6562.86 ($2p$-$3s$), 6562.74 ($2s$-$3p$), and 6562.81 Å ($2p$-$3d$). Under higher resolution there are seven lines. The maximum separation is 120 mÅ and shows the difficulty of determining the slow atom energy distribution from H_α line profiles.

DISCUSSION

We have measured the line profile of H L_β for the first time and compared it to a higher-resolution line profile of H L_α. The resolution was sufficient to determine the kinetic-energy distribution function of fast H($3p$) atoms from an analysis of the blue wing at 100-eV impact energy. The kinetic-energy distribution function shows that the Q_1 states are most important for H($3p$) production, whereas Q_2 states are more significant for H($2p$) production. Accurate analysis of the slow energy peak requires higher-resolution studies of the line central peak. Preliminary results from our measurement indicate a line FWHM of less than 30 mÅ and a kinetic-energy distribution with peak energy between 0 and 1 eV. The quantum yield of fast and slow atoms released in the various types of dissociation processes is 0.53 for slow atoms and 0.47 for fast atoms. A comparison of the fast kinetic-energy distribution for H($3p$) from this experiment to that for H($3s$,$3p$,$3d$) of Ogawa and co-workers shows that they are very similar. This result suggests that the three H_α multiplets have the same line profile at 100-eV electron-impact energy.

Our direct measurements of the H L_β cross section at 100-eV electron-impact energy by two different methods are in very good agreement with one another and yield an absolute cross section of $(3.2\pm0.8)\times10^{-19}$ cm^2. Due to blending with nearby L & W bands, this measurement required an estimate of the profile of the red wing. We assumed the line profile was symmetric, which causes about 10% uncertainty in the cross section. We can extend the absolute cross-section result at 100 eV to other energies by normalizing the low resolution H_α cross-section results of Karolis and Harting [7] from 0–105 eV and of Freund *et al.* [16] beyond 100 eV. This result is shown in Fig. 4. The excitation function indicates the four thresholds found by Karolis and Harting at 16, 26, 35, and 43 eV. Recently, from high-resolution studies of the excitation function of the H_α wing, Ogawa *et al.* [3] found thresholds at 22–23 and 27 eV. In addition, we show

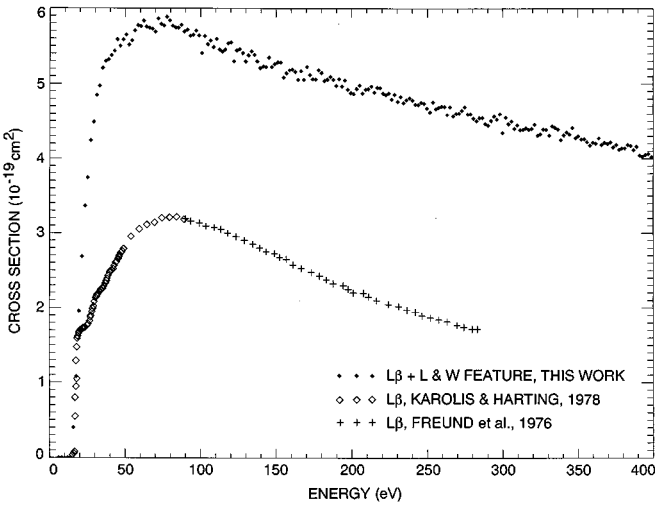

FIG. 4. Estimated absolute cross section of H L_β from published optical excitation function measurement of H_α. The excitation function measurements of Karolis and Harting [7], shown as open diamonds from 0–100 eV, and Freund *et al.* [16], shown as plus signs from 100–290 eV, are normalized to the 100-eV cross section of H L_β from this work. The cross section of the blended H L_β and L & W feature from this work is shown as a filled square.

in Fig. 4 the cross section for the entire blended feature of Fig. 1, including H L_β and L & W features of Table I. The cross section of the blended feature is $(5.69\pm0.80)\times10^{-19}$ cm^2 at 100 eV. The peak cross section for both excitation functions in Fig. 4 occur near 80 eV.

Our previous indirect estimate of the H L_β cross section of 8.3×10^{-19} cm^2 at 100 eV was based on the $3s$, $3p$, and $3d$ excitation rates of Julien, Glass-Maujean, and Descoubes [21] and Glass-Maujean [22]. However, the excitation rates were measured at threshold (near 16.56 eV) and may change at higher energy. Additionally, these authors have measured the velocity distribution of fast and slow atoms, using measurements of anticrossing signals between Zeeman sublevels. They have detected slow atoms with energies between 0.3 and 0.4 eV and fast atoms with energies of ~10 eV in good agreement with the results for fast atoms presented here. The Doppler shift [21,22] for the slow atoms corresponds to ~30 mÅ, also in excellent agreement with our estimate.

Recent studies of H_2 photodissociation with synchrotron radiation have shown the angular-momentum population of $3l$ varies strongly with photon energy, particularly in the region of predissociation peaks [23]. On the other hand, at high photon energy the angular-momentum substates tend to converge to equal population.

We can also make an estimate of the contribution of $3p$ atoms to the H_α cross section and to the total $3l$ emission cross section. The branching ratio, ω_{1s3p}, for $1s$-$3p$ emission is 0.881. The emission cross section for $3p$ at 100 eV can be found to be $Q_{1\beta}/\omega_{1s3p}=3.6\times10^{-19}$ cm^2. We sum the H($3p-1s$) cross section found in this study (3.2×10^{-19} cm^2) with the H($3l$-$2l$) cross section (9.3×10^{-19} cm^2) [7]. On this basis, we estimate that the $3p$ atoms contribute $29\pm10\%$ of the total $3l$ emission cross section of 12.5×10^{-19} cm^2 [7]. This fractional percentage indicates that there is probably no

preferential population of $3s$, $3p$, and $3d$ sublevels. The H_α radiation is nearly the sum of the cross sections for $H(3s)$ and $H(3d)$ dissociation. At 100 eV, our results show that the $3p$ cross-section contribution to H_α is 4.6%, in agreement with earlier conclusions by Vroom and de Heer [24]. Vroom and de Heer also indicate an upper limit to $H(3p)$ dissociative cross section of 3.57×10^{-19} cm^2 at 50 eV. The cross section plot in Fig. 4, together with the $1s$-$3p$ branching ratio, can be used to give the $H(3p)$ cross section of 3.2×10^{-19} cm^2 at 50 eV.

ACKNOWLEDGMENTS

The research described in this text was carried out at the Jet Propulsion Laboratory, California Institute of Technology. The work was supported by the U.S. Air Force Office of Scientific Research (AFOSR), the Aeronomy Program of the National Science Program (Grant No. ATM-9320589 to the University of Southern California), and NASA Planetary Atmospheres, Astronomy/Astrophysics, and Space Physics Program Offices. S. M. Ahmed and X. Liu are supported by the National Research Council.

[1] K. Ito, N. Oda, Y. Hatano, and T. Tsuboi, Chem. Phys. **17**, 35 (1976).
[2] M. Higo, S. Kamata, and T. Ogawa, Chem. Phys. **73**, 99 (1982).
[3] T. Ogawa, Y. Jinbou, N. Yonekura, K. Furuya, and K. Nakashima, Bull. Chem. Soc. Jpn. **66**, 3506 (1993).
[4] J. M. Ajello, S. M. Ahmed, I. Kanik, and R. Multari, Phys. Rev. Lett. **75**, 3261 (1995).
[5] J. M. Ajello, I. Kanik, S. M. Ahmed, and J. T. Clarke, J. Geophys. Res. **100**, 26411 (1995).
[6] X. Liu, S. M. Ahmed, R. A. Multari, G. K. James, and J. M. Ajello, Astrophys. J. Suppl. **101**, 375 (1995).
[7] C. Karolis and E. Harting, J. Phys. B **11**, 357 (1978).
[8] J. M. Ajello, D. Shemansky, T. L. Kwok, and Y. L. Yung, Phys. Rev. A **29**, 636 (1984).
[9] J. T. Clarke, L. Ben Jaffel, A. Vidal-Madjar, G. R. Gladstone, J. H. Waite, R. Prange, J. Gerard, J. Ajello, and G. James, Astrophys. J. Lett. **430**, L73 (1994).
[10] J. T. Clarke, G. R. Gladstone, and L. Ben Jaffel, Geophys. Res. Lett. **18**, 1935 (1991).
[11] J. M. Ajello *et al.*, Appl. Opt. **27**, 890 (1988).
[12] H. Abgrall, E. Roueff, F. Launay, J.-Y. Roncin, and J.-L. Subtil, J. Mol. Spectrosc. **157**, 512 (1993).
[13] H. Abgrall, E. Roueff, F. Launay, J.-Y. Roncin, and J.-L. Subtil, Astron. Astrophys. **101**, 273 (1993).
[14] H. Abgrall, E. Roueff, F. Launay, J.-Y. Roncin, and J.-L. Subtil, Astron. Astrophys. **101**, 323 (1993).
[15] W. H. Press, B. P. Flannery, S. A. Teukolsky, and W. T. Vettering, *Numerical Recipes* (Cambridge University Press, Cambridge, England, 1987).
[16] R. S. Freund, J. A. Schiavone, and D. F. Brader, J. Chem. Phys. **64**, 1122 (1976).
[17] S. R. Ryan, J. J. Spezeski, O. F. Kalmam, W. E. Lamb, L. C. McIntyre, and W. H. Wing, Phys. Rev. A **19**, 2192 (1979).
[18] J. M. Ajello, D. E. Shemansky, and G. K. James, Astrophys. J. **371**, 422 (1991).
[19] T. Ogawa and M. Higo, Chem. Phys. Lett. **65**, 610 (1979).
[20] S. L. Guberman, J. Chem. Phys. **78**, 1404 (1983).
[21] L. Julien, M. Glass-Maujean, and J. P. Descoubes, J. Phys. B **6**, L196 (1973).
[22] M. Glass-Maujean, J. Phys. B **11**, 431 (1978).
[23] N. Terazawa, N. Kouchi, M. Ukai, K. Kameta, Y. Hatano, and K. Ito, J. Chem. Phys. **100**, 7036 (1994).
[24] D. A. Vroom and F. J. de Heer, J. Chem. Phys. **50**, 580 (1969).
[25] X. Liu (unpublished).
[26] S. L. Guberman (private communication).